# Spectral Variability and Discrimination Assessment in a Tropical Peat Swamp Landscape Using CHRIS/PROBA Data

**Veraldo Liesenberg[1]**
*Remote Sensing Group, Institute of Geology,*
*Freiberg University of Mining and Technology,*
*B.-v-Cottastr. 2, 09599, Freiberg, Germany*

**Hans-Dieter Viktor Boehm**
*Kalteng Consultans, Remote Sensing of Kalimantan,*
*Kirchstockacher Weg 2, 85635, Hoehenkirchen, Germany*

**Richard Gloaguen**
*Remote Sensing Group, Institute of Geology,*
*Freiberg University of Mining and Technology,*
*B.-v-Cottastr. 2, 09599, Freiberg, Germany*

**Abstract:** In this study, we examine seasonal aspects and the potential of multi-angle CHRIS/PROBA data, acquired at two different dates, to improve forest classification. The test site is a typical peat swamp landscape located in Central Kalimantan, Indonesia. We focus on eight specific land use/cover categories from a single view angle and from a multi-angular perspective. We show that: (1) reflectance changes from the end of the monsoon to the beginning of the dry season in the visible were small and slightly positive for the forestry classes, whereas slightly negative for grassland classes; (2) reflectance increases according to the successional stages for a given angle and were higher in the beginning of the dry season; (3) reflectance values increase in the near-infrared with decreasing leaf area index (LAI); and (4) classification results using a multi-angular approach were statistically better at a 5% level of significance from a single view approach on both selected dates, showing that anisotropy information can improve differentiation between peatland landscape classes.

## INTRODUCTION

The ability of different multi-angular instruments to obtain quasi-simultaneous multispectral measurements at different view angles has brought new perspectives to vegetation mapping and to the quantification of biophysical properties of the canopy structure (Diner et al., 1999). Compared to nadir-viewing sensors, multi-angular

[1]Corresponding author; email: veraldo@gmail.com

measurements explore the reflectance anisotropy that is described by the bidirectional reflectance distribution function (BRDF).

The BRDF describes the reflectance anisotropy of a given target as a function of both illumination and viewing geometry. It depends on wavelength and is determined by the intrinsic surface properties (Kimes et al., 1994; Schill et al., 2004; Schaepman-Strub et al., 2006). Changes that occur in the reflectance due to anisotropy effects may be useful for improving the classification accuracy of land cover classes in different environments.

The Compact High Resolution Imaging Spectrometer (CHRIS) was launched on October 21, 2001 as a technology demonstrator on the Project for On Board Autonomy (PROBA) (Barnsley et al., 2004). PROBA is a small platform and can acquire up to 62 spectral bands in the 400-1050 nm range with a spectral resolution of 5–12 nm. The CHRIS/PROBA system allows different acquisition modes in terms of both spectral channels and spatial resolution, with a nominal ground resolution between ~17 and 34 m. Five principal modes have been selected according to the five major applications: aerosol, land cover, vegetation, coastal zones, and water bodies. Due to its four reaction wheels, the CHRIS sensor acquires nearly simultaneous images at times when its zenith angle is close to a set of along-track fly-by zenith angles at ±0°, ±36°, and ±55°. The nominal swath is 14 km.

Although different investigations have been made to evaluate the ability of multi-angular CHRIS/PROBA data for vegetation studies, they were mostly restricted to non-tropical environments (e.g., Guanter et al., 2005). Therefore a better understanding of how sunlight is scattered as a function of seasonality and sun zenith angle at distinct view angles in tropical rain forest is still necessary.

Natural tropical peat swamp forests are important for their rich biodiversity and as a carbon pool (Page et al., 2002; Jauhiainen et al., 2005; Jaenicke et al., 2008). However, peat swamp forests are decreasing due to deforestation, conversion into farm land, excessive drainage, the use of shifting cultivation on a large scale, illegal logging, and forest fires. Remote sensing data can provide useful information in such environments for hydrological and wildfire modeling, retrieval of biophysical parameters, and the management of natural resources (Twelle et al., 2008; Reif et al., 2009; Wijaya et al., 2010).

In this study, two CHRIS acquisitions (mode 3) collected over a peat swamp landscape in Central Kalimantan, Indonesia) were evaluated as a function of the viewing geometry (anisotropy) and seasonality for selected land cover classes. To demonstrate the sun-view effects on the discrimination of a typical peat swamp forest succession, the images were also evaluated for classification purposes.

## STUDY AREA DESCRIPTION

The study area is a 14 km × 14 km tract (subset result) located close to Palangkaraya, the capital of Central Kalimantan province, between the Sabangau and Kahayan rivers (Fig. 1). The site has a humid tropical climate (type Af in the Köppen system) with an annual rainfall of 3500 mm and an annual mean air temperature of 25° C. There is a dry season from May to October and a monsoon from November to April. The area is quite flat, and the maximum altitude is 30 m above sea level. According to Hirano et al. (2007) the average peat thickness of the study area is 4 m.
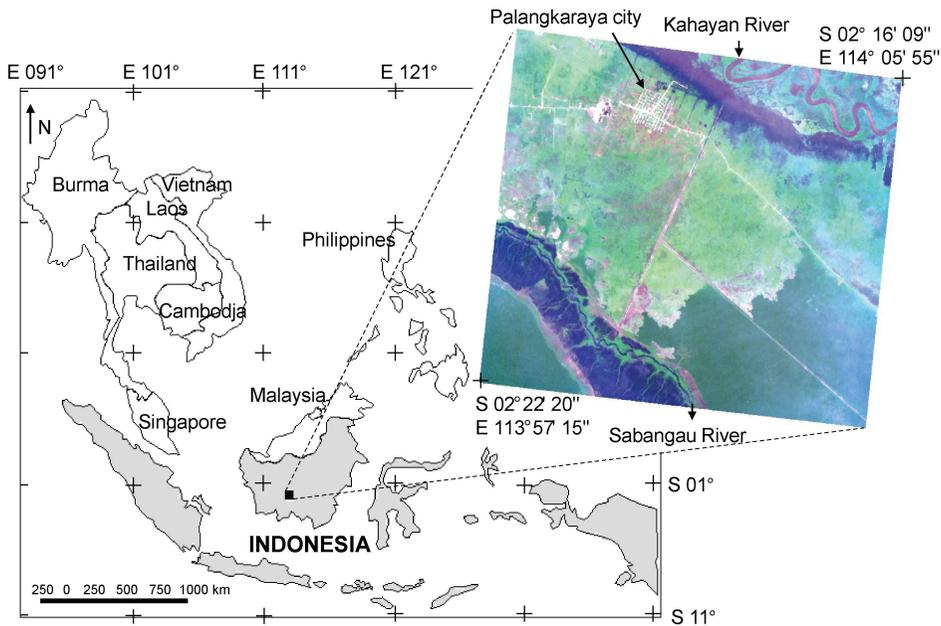
**Fig. 1.** Location of the study area in Central Kalimantan (southern island of Borneo, Indonesia) with detail regarding the true color composition of the CHRIS/PROBA image at nadir viewing and acquired on May 18, 2004. Arrows indicate the Kahayan and Sabangau rivers and the city of Palangkaraya.
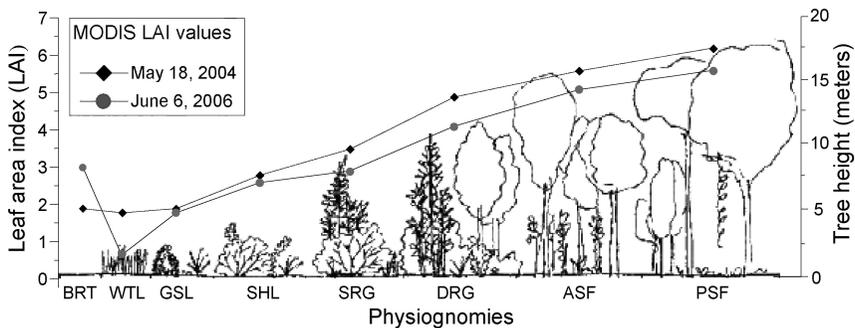


**Fig. 2.** Gradient of the selected classes under study with details of average tree height and the MODIS Level 2 leaf area index (LAI) product. Graphic illustration of the physiognomies was modified from Boehm et al. (2005). Classes: PSF = peat swamp forest; ASF = advanced secondary forest: DRG = dense regrowth; SRG = sparse regrowth; SHL = shrubland; GSL = grassland; WTL = wetland; BRT = burned areas.

The study site is located in Block C of the Mega Rice Project. A canal runs through the forest for drainage. There are also large areas of devastated peatlands, resulting in the permanent partitioning of the forest into different degrees of succession. According to Hirano et al. (2007) the leaf area index (LAI) of peat swamp forest
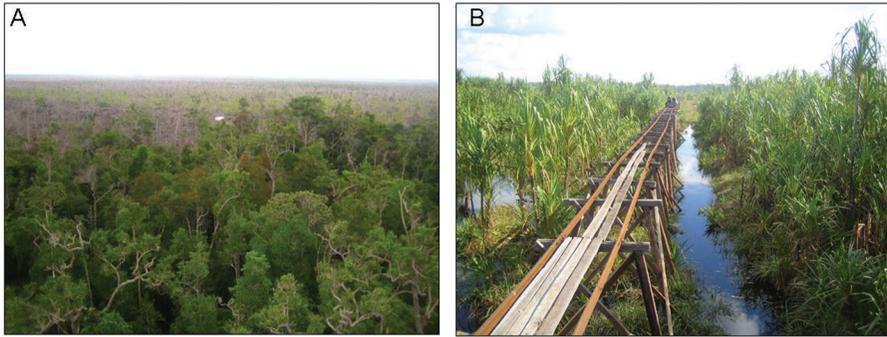
**Fig. 3.** Pictures taken over (A) peat swamp forest from a meteorological flux tower and (B) wetland from a railway used in the past for logging activities.
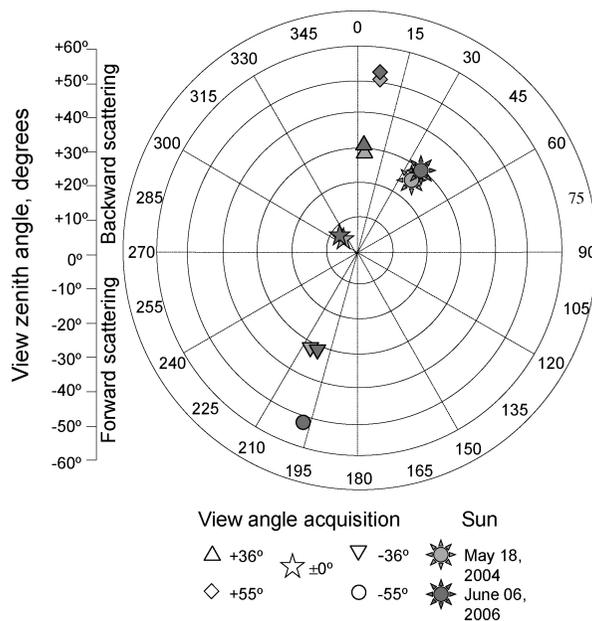


**Fig. 4.** Geometry of CHRIS/PROBA data acquisition over the study area represented in a polar graphic. Different grey tones indicate different time acquisitions and view angles.

here in the monsoon is close to 6, typical for areas of advanced and dense tropical rain forest and in agreement with the MODerate Imaging Spectroradiometer (MODIS) Level 2 LAI product (Fig. 2). Areas of pasture, small agricultural fields, small villages, and forest degraded by selective logging can be also observed.

According to Boehm et al. (2005) the peat swamp environment within the study area is divided into eight classes: (1) Peat Swamp Forest (henceforth PSF); (2) Advanced Secondary Forest (ASF); (3) Dense Regrowth (DRG); (4) Sparse Regrowth (SRG); (5) Shrubland (SHL); (6) Grassland (GSL); (7) Wetland (WTL); and (8) Burned Areas
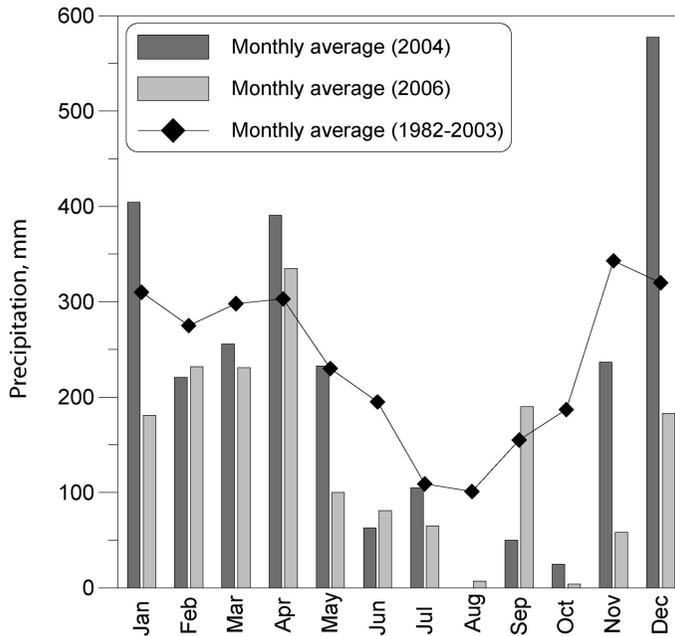
**Fig. 5.** Monthly average precipitation values for the study area in 2004, 2006, and based on historical measurements from 1981 to 2003. Precipitation measurements were collected from a meteorological flux tower located inside the study area. Historical precipitation values were based on Usup et al. (2004).

(BNT). To give a better idea of the different physiognomies in the study area, Figure 2 displays a schematic vegetation sketch highlighting biophysical properties. Extreme physiognomies are further detailed in Figure 3.

Dominant tree species in the emergent tree layer of PSF are *Combretocarpus rotundatus*, *Cratoxylum arborescens*, *Buchanania sessifolia*, and *Tetramerista glabra* (Page et al., 1999; Brearley et al., 2004). Shrubs, including young trees of the dominant species, grow beneath the emergent layer. The average canopy height is ca. 20 m. The forest floor is covered with thick tree debris, dominantly leaf litter, and is uneven with hummocks and hollows (Jauhiainen et al., 2005).

**METHODS**

**Image Acquisition and Pre-processing**

The geometry of the CHRIS/PROBA image collected over the study area is shown in Figure 4. The images were acquired under a very clear sky at 3:11 a.m. GMT, May 18, 2004, at the end of the monsoon and with one-sixth cloud cover at 3:04 a.m. GMT, June 06, 2006, at the beginning of the dry season. Because there was an abnormal rainfall pattern in 2004 and 2006 (Fig. 5), some seasonal effects were observed in the images.

Data were collected in mode 3 (Land) in an oblique solar plane condition at visible and near infrared wavelengths in 18 bands (Table 1). The Ground Instantaneous

**Table 1.** Center Wavelength and Full Width at Half Maximum (FWHM) of the CHRIS Spectral Bands

| Band number | May 18, 2004 | | June 06, 2006 | |
|---|---|---|---|---|
| | Wavelength, nm | FWHM | Wavelength, nm | FWHM |
| 1 | 441.4 | 12.1 | 442.5 | 10.5 |
| 2 | 490.0 | 11.6 | 490.3 | 11.6 |
| 3 | 529.8 | 11.5 | 530.2 | 11.5 |
| 4 | 551.1 | 12.9 | 551.5 | 12.9 |
| 5 | 569.7 | 10.7 | 570.2 | 10.7 |
| 6 | 631.0 | 14.0 | 631.6 | 14.0 |
| 7 | 660.7 | 15.7 | 661.5 | 15.8 |
| 8 | 674.1 | 11.0 | 674.9 | 11.0 |
| 9 | 696.9 | 11.9 | 697.8 | 11.8 |
| 10 | 706.0 | 6.0 | 706.8 | 6.1 |
| 11 | 712.1 | 6.2 | 712.9 | 6.2 |
| 12 | 741.2 | 13.5 | 742.1 | 13.5 |
| 13 | 751.5 | 6.9 | 752.5 | 6.9 |
| 14 | 780.3 | 22.4 | 781.4 | 22.5 |
| 15 | 871.5 | 27.4 | 872.7 | 27.4 |
| 16 | 894.7 | 18.9 | 896.1 | 19.0 |
| 17 | 909.0 | 9.7 | 910.5 | 9.8 |
| 18 | 1018.2 | 43.7 | 1019.7 | 43.7 |

Field of View (GIFOV) was close to 20 m at nadir. This high spatial resolution allows a better assessment of the anisotropy at physiognomy level than other available sensors at orbital level (Diner et al., 1999). On May 18, 2004, images were acquired only at four different nominal view zenith angles due to failure in data acquisition at –55°. In this study, negative and positive view angles represent the forward and backward scattering direction with the predominance of shadowed and sunlit canopy components viewed by the sensor, respectively.

Striping effects were reduced by replacing abnormal horizontal lines with the average response of adjacent lines. Radiance data were converted to surface reflectance anisotropy (hemispherical directional reflectance factor, HDRF) (Schaepman-Strub et al., 2006) using the Fast Line-of-Sight Atmospheric Analysis of Spectral Hypercubes (FLAASH) algorithm. FLAASH is based on a MODTRAN4 approach for path-scattered radiance, absorption, and adjacency effects for nadir and non-nadir viewing instruments (Felde et al., 2003). Because the HDRF approximation produced by FLAASH includes a hemispherical and adjacency component, the approximation with the bidirectional reflectance factor (BRF) is valid, at least in terms of its trend (Abdou et al., 2000; Schill et al., 2004). Input data for the radiative transfer code were
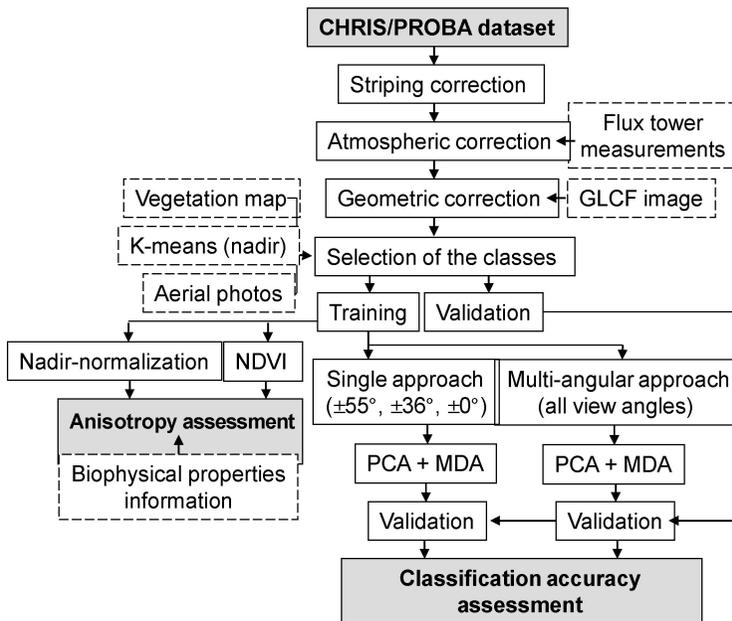
**Fig. 6.** Schematic diagram of the processing flow applied to this study.

collected by instruments in a tower maintained by the Asia Flux Network inside the study area (Hirano et al., 2007).

Geometric correction was performed using a set of 20 ground control points (GCPs) extracted from a master image—i.e., a georeferenced Landsat scene available from the Global Land Cover Facility (GLCF). A polynomial method of one degree and the nearest neighbor resampling process were selected. GCPs were collected over visible features presented in the images such as roads, irrigation canals, and small logged patches inside the forest. Values of root mean-square error (RMSE) for 2004 images were as follows: 28.8 m at –55°, 24.2 m at –36°, 14.8 m at nadir and 30.2 m at +36°, whereas for 2006 the corresponding figures were 39 m at –55°, 29.2 m at –36°, 21.6 m at nadir, 29.8 m at +36° and 36.4 m at +55°. However, even after geometric correction there was a need for small adjustments in the location of sample plots due to pixel distortion at extreme viewing.

**Data Analysis**

A methodology flowchart is shown in Figure 6. Following the pre-processing steps described previously, the first step in the data analysis of the CHRIS HDRF dataset was the selection of pixels in homogeneous areas representative of the land cover types illustrated in Figure 2. The classes under study have a very important spatial distribution in the peat swamp domain in Central Kalimantan (Nishimua et al., 2007). Anisotropic assessment at the physiognomic level was only possible due to the high spatial resolution of CHRIS/PROBA. Class election was based on the combined analysis of available vegetation maps (e.g., Boehm et al., 2005), K-means unsupervised

classification results derived from nadir CHRIS data, and aerial photograph interpretation collected simultaneously during a Light Detection And Ranging (LiDAR) field campaign conducted by Kalteng Consultants and Milan Geoservice GmbH.

For each physiognomic class, 440 pixels (40 pixels as training and 400 pixels as validation) were selected with approximately similar positions on each dataset. The exception was for the image collected in 2006 where only a training dataset was considered due to the presence of clouds and image overlapping. For pixel selection only well delimited areas in the different view-angle images were sampled to represent the eight classes under study. Special attention was given to avoid spatial correlation between neighboring pixels. To characterize spectral-angular variations of the classes, the training dataset was plotted in each view angle and date. The angular response of each view angle was normalized against its correspondent nadir value and date (e.g ±36°/nadir and ±55°/nadir). View-angle effects on the normalized difference vegetation index (NDVI = [near-infrared minus red]/[near-infrared plus red]) were also analyzed.

CHRIS/PROBA were plotted as a function of the view angle and related to MODerate resolution Imaging Spectroradiometer (MODIS) Level 2 Land Surface Products such as leaf area index (LAI) acquired close to the CHRIS/PROBA acquisitions. Further analysis of CHRIS data also consisted of the application of Principal Components Analysis (PCA). An example of the use of PCA, including the equations used to obtain the eigenvalues, eigenvectors, and the principal component (PC) scores, may be found in Jensen (2005). In the present study PCA, was applied over the training dataset using the HDRF values as input variables for each view angle. A correlation matrix derived from the reflectance values provided the basis for the eigenvalue and eigenvector calculations and for the subsequent determination of the PC scores. Each score represents a transformed spectrum from the linear combination of the reflectance of the bands. By analyzing the eigenvectors and the PC score differences, the contribution of each band to the variability in the dataset and the spectral similarity between the land covers at each view angle could be established.

The last step in data analysis was to use the validation pixel dataset to evaluate the view-angle effects on the classification of the selected land use classes for the image collected in 2004 (clear sky condition). For the image acquired in 2006, the leave-one-out procedure was used for classification purposes (Huberty, 1984). Two approaches were used in the data analysis of both dates: single (analysis at each view angle separately) and multi-angular (combination of all view angles).

In both approaches, PCA scores provide input variables for Multiple Discriminant Analysis (MDA). MDA performs linear discriminant analysis for multiple groups, with the final objective of assigning samples to specific groups. This technique was used to provide multi-group maximal separability, classification, and feature selection. PCs with eigenvalues greater than 1 were retained and their scores used for MDA. To evaluate data normality the Kolmogorov-Smirnov test was used. A stepwise procedure was applied to select the best retained PC scores and to maximize the Mahalanobis distance between the two most similar classes.

The probability of $F$ was used as a criterion to include (0.05) and exclude (0.10) variables. The validation dataset (400 pixels for each class) was then used to test the ability of the resulting discriminant function to classify new pixels. In the second approach (multi-angular), the PCA was applied over all datasets (four view angles

for 2004 and five for 2006). The total set of retained PC scores was then used as the input candidate variables for the MDA and the best variables were selected from the stepwise discrimination procedure.

Finally, the accuracy of the classification results from the MDA using the set of validation pixels was compared between the single and multi-angular approaches at each date. For classification accuracy assessment, an error matrix was prepared and the overall accuracy was calculated by comparing the classification results and the validation dataset. The overall accuracy is the percentage of the correctly classified pixels in the validation dataset. The kappa coefficient was also computed as a measure of the difference between the actual agreement and the change agreement. The statistical significance of differences in classification accuracy statistics was evaluated using both the *Z* and McNemar tests (Congalton and Green, 1999).

### RESULTS AND DISCUSSION

**Angular Sensitivity of Peatland Classes**

CHRIS-derived surface reflectance anisotropy between different peatland classes is shown in Figure 7 for two extreme view angles (–36° and +36°) and two distinct dates (end of the monsoon and beginning of the dry season). To facilitate the graphic representation, results are presented for only three of the eight classes under study. In both figures, the view angles at –36° (forward scattering) represent spectra with higher reflectance values than those observed in the backward scattering direction (+36°) and +55° viewing angles (result not shown). This behavior is due to the prevalence of sunlit-view canopy components. When the sensor moved away from the backward direction, reflectance decreased because of the increase in the relative proportion of the shadowed-view canopy components. Wetland as an exception showed a specular reflectance at –36° (result not shown) at the end of the monsoon.

For a given view angle and date, the near infrared reflectance increased from burnt areas to shrub, grassland to peat swamp forest (PSF), and then to the successional stages. The successional stages also revealed large reflectance values in this spectral region with decreasing biomass (e.g., LAI) (Fig. 2). Due to their canopy architecture and shadow introduced by three to four structured canopy layers, the peat swamp forest showed the strongest absorption, followed by the ASF in the red band.

The blue band shows higher reflectance values in the backscattering direction domain than at nadir and the forward scattering suggests a coupled effect of mixed spectral properties of the vegetation itself and the atmosphere. Atmospheric dispersion in the blue region is still very difficult to remove at the backward scattering direction (e.g. +36°; Fig. 7). Such behavior was previously noticed by Xavier and Galvão (2005) in the western Amazon using Multiangle Imaging SpectroRadiometer (MISR) on board the Terra platform and by Galvão et al. (2009) in the eastern Amazon using hyperspectral CHRIS/PROBA data. In such environments, the plane-parallel assumptions of the radiative transfer code for tropical atmosphere mode may start to fail.

Reflectances are quite similar at nadir between dates. The spectral behavior detected by the multispectral mode of CHRIS/PROBA between peat swamp forest and successional stages (e.g., ASF, DRG, and SRG; Fig. 2) is in agreement with previous investigations conducted in distinct tropical environments in the Amazon biome
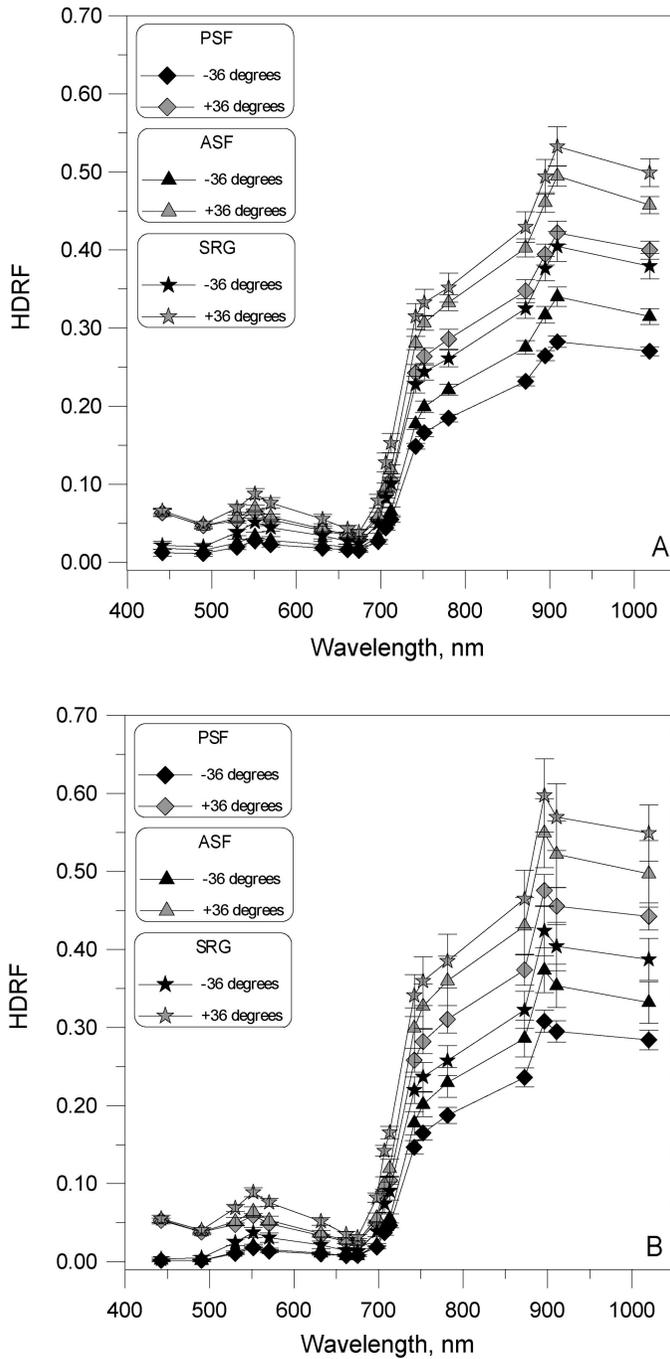
**Fig. 7.** CHRIS/PROBA reflectance anisotropy of some peatland cover classes in the forward (–36° view angle) and backward (+36° view angle) scattering directions in (A) 2004 and (B) 2006 respectively. Average and standard deviation of 40 pixels. Refer to Figure 2 for the selected class's category.
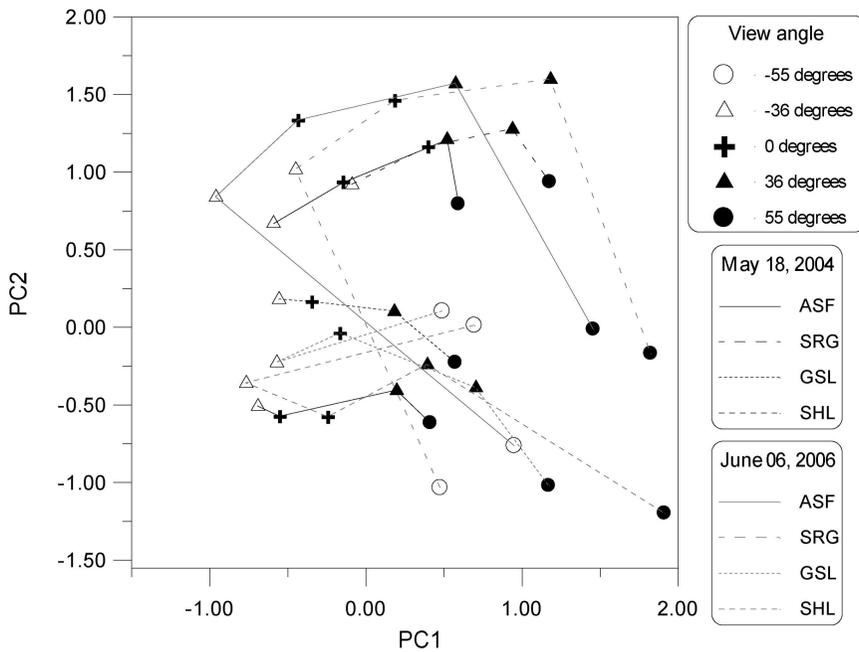
**Fig. 8.** First two principal components scores (PC1 and PC2; average of 40 pixels) as a function of the view-angle acquisition in May 18, 2004 and June 06, 2006 for four distinct land cover types. Crossed, closed, and open symbols indicate nadir viewing, and backward and forward scattering directions, respectively. Refer to Figure 2 for the selected class's category.

by Foody et al. (1996), Kimes et al. (1999) and Lu et al. (2003) using Landsat data and more recently by Galvão et al. (2009) using the hyperspectral mode of CHRIS/PROBA data. Despite this behavior, confusions due to both environmental and historical aspects that are sometimes difficult to characterize often occur when trying to discriminate between successional stages (Lu, 2005; Vieira et al., 2003).

A better understanding of the spectral-angular variations associated with the selected land covers was obtained from the inspection of the PCA results. The projection of the average scores (average of the training dataset for four land cover types and view angles) along the first two principal component axes (PC1 and PC2) is displayed in Figure 8. To allow a better graphic representation, results were presented for only four classes per date. Open and closed symbols linked by a single line indicate spectra for a given land cover collected in the forward and backward scattering directions, respectively. The angular response presented in Figure 8 could be divided into two general groups with biomass variations (e.g., LAI). The first group is related to forestry classes that have similar shape in PC space over time (e.g., ASF, DRG) due to higher LAI values (Fig. 2). The second group was related to classes with lower LAI values and higher soil ground contribution (e.g., GSL and SHL). Similar patterns were also obtained by Zhang et al. (2002) and Xavier and Galvão (2005), which demonstrated similarities between angular signatures for distinct groups of land covers and their relationship with different biomes and biophysical properties.

The mean reflectance over the spectral bands (brightness) tends to increase to the right side of the PC1 axis except at −55° in the dry season (Fig. 8). The red-edge reflectance and near-infrared/red reflectance ratio tends to increase from the bottom to the top of the PC2 axis to the end of the moonson and the beginning of the dry season. Thus mean reflectance tends to increase from the grassland classes (low PC2 scores in Fig. 8; low LAI values) to the forestry classes (high PC2 scores in Fig. 8; high LAI values) and from −36° to extreme viewing for all classes (Fig. 8).

An increase in brightness was particularly marked in the backward scattering direction (positive values in Fig. 7) due to the predominance of sunlit-view vegetation components. At +36° the forestry classes presented higher mean reflectance than the grassland classes (e.g. GSL and SHL). In general the spectral variability of the mean reflectance increased from nadir to extreme view angles for all selected land covers.

Figure 9 displays the trend and magnitude in phenologic patterns across peat swamp forest and burned areas, obtained by subtracting the HDRF image from May 18, 2004 from the HDRF image from June 06, 2006. In contrast, dry-season changes in visible reflectance are small and slightly positive for the forestry classes (e.g. PSF; Fig. 9A), and slightly negative for grassland classes (e.g., burned areas; Fig. 9B). The slight increase in NIR reflectance observed in the peat swamp forest may be related to leaf flushing and leaf exchange (Fig. 9A; Huete et al., 2006), whereas the strongly positive NIR values for burned areas (Fig. 9B) largely reflects regeneration effects (Vieira et al., 2003). Indeed the LAI increased from 1.9 to 3 during the acquisition time of both scenes. According to Huete et al. (2006), leaf flushing and leaf exchange occur with seasonal peaks in sunlight during the dry season in tropical environments.

The sun zenith angle variation between dates may also influence the seasonal canopy spectral profiles through shading and illumination effects. Such variation becomes smaller in the dry season and canopy shading may increase. This may also contribute to the observed increases in reflectance, particularly in the NIR. In general there are strong optical-phenologic differences as well as with associated sun-view-angle effects among the classes, and they are related to vegetation type and disturbance history (Vieira et al., 2003). In peatland environments, temperatures are slightly warmer and evaporation is higher in the dry season, as the soil water level is very shallow. This prevents drying of the herbaceous layer in grassland classes as well as its vulnerability to strong drought effects compared to other tropical rain forest environments (Huete et al., 2008). Lucas et al. (1993) and Carreiras et al. (2006) also report that phenologic information may be useful for mapping tropical environments, suggesting an improvement when this additional source of data is considered in classification analysis.

To demonstrate the angular sensitivity of some classes under study, the nadir-normalized red and near-infrared reflectance values were obtained (Fig. 10). The strongest differences from the nadir were noticed in the backward-scattering direction (positive view angles) with the predominance of illuminated vegetation components for the sensor. The red band presented a more anisotropic behavior than the near-infrared band, as indicated by the wider range of normalized HDRF data in the backward direction (Fig. 10). This result is in agreement with that observed by Sandmeier and Deering (1999).

According to Sandmeier and Deering (1999) the directional effects are particularly strong in spectral regions of high absorbance such as the red chlorophyll interval, mainly for peat swamp forest and grassland. However, directional effects were
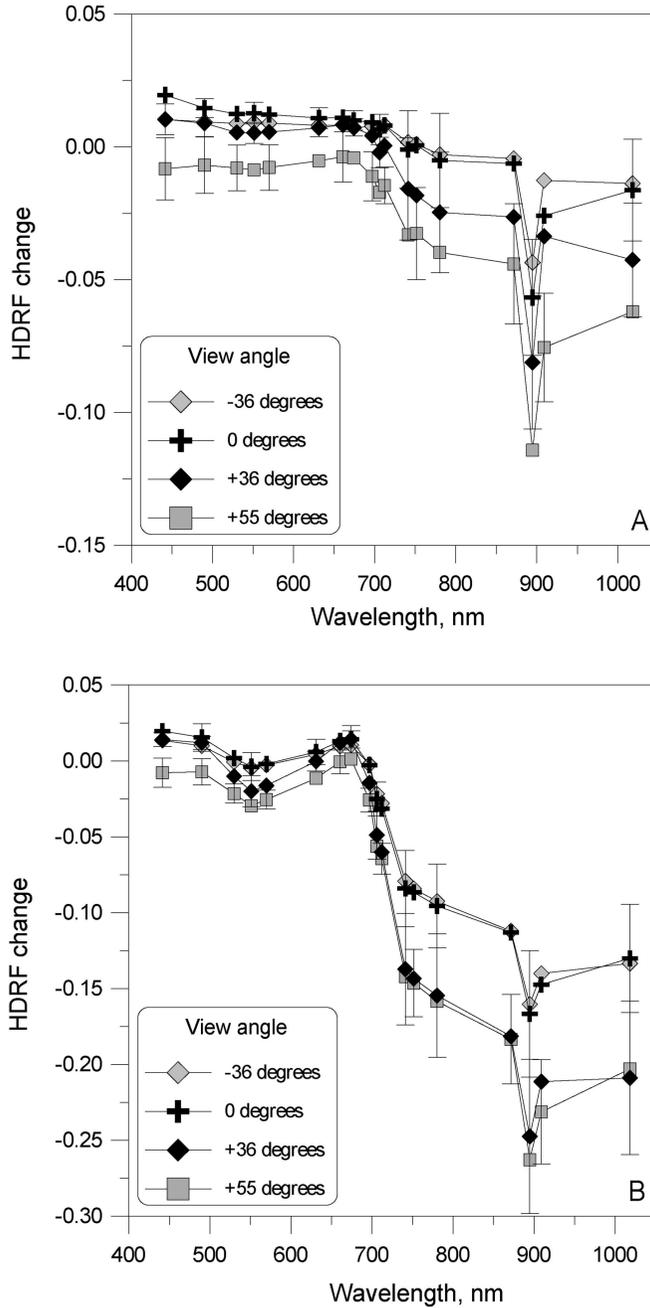
**Fig. 9.** Subtraction of HDRF images acquired on May 18, 2004 and June 06, 2006 for (A) peat swamp forest, and (B) burned areas. Average and standard deviation of 40 pixels. Negative values indicate increasing reflectances. Positive values represent reflectance decreases through the dry season. Refer to Figure 2 for the selected class's category.
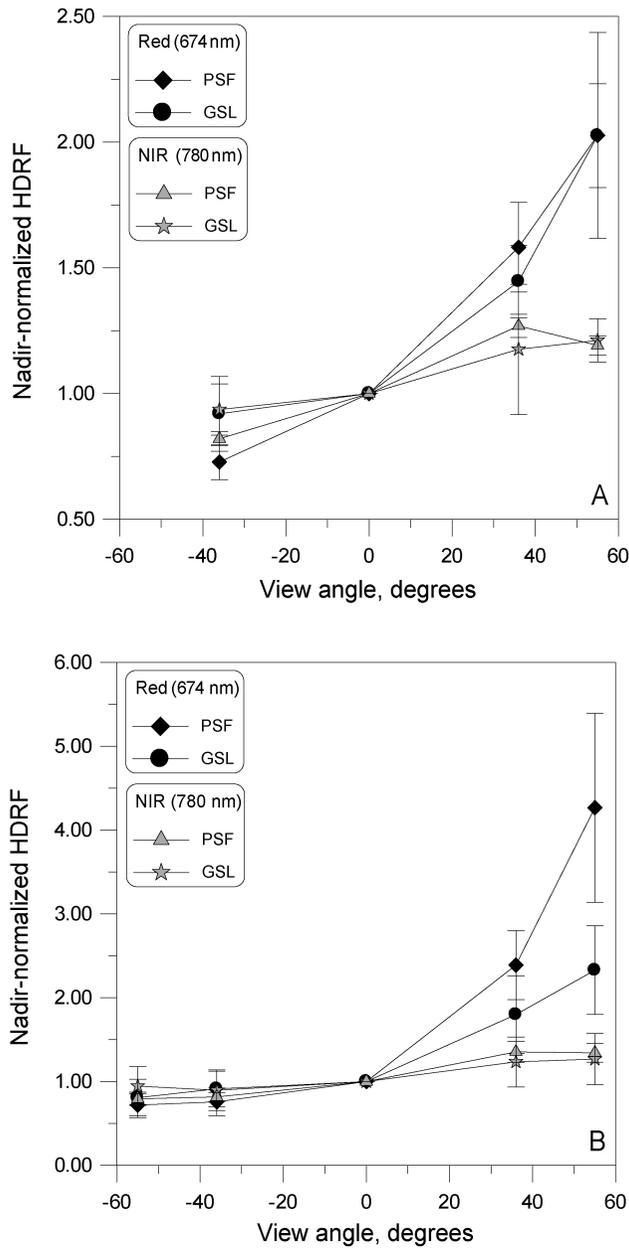
**Fig. 10.** Angular variations in nadir-normalized reflectance of different tropical peat swamp classes for selected red (674 nm) and near-infrared (780 nm) bands in (A) May 18, 2004 and (B) June 06, 2006. Average and standard deviation of 40 pixels. Refer to Figure 2 for the selected class's category.

less pronounced at extreme viewing in the near-infrared due to the predominance of multiple scattering processes that reduce the spectral contrast between shaded and illuminated components (Sandmeier et al., 1998). Thus the direction of maximum

reflectance for the backward scattering direction at the near-infrared region was better defined for classes with higher LAI values (e.g., PSF) than classes with lower LAI values (e.g., GSL) at the end of the monsoon.

Directional effects are also noticed after the determination of NDVI (Fig. 11). NDVI variations in distinct view angles were stronger for Shrubland than for the remaining classes and decreased for the forest classes. In general NDVI decreases from nadir to extreme view angles for these forest types due to the relatively stronger increase in their red response than in their near-infrared reflectance, especially in the backward scattering direction in both dates (Fig. 11). However, NDVI values increase toward extreme viewing for Shrubland due to the relative increase in its near-infrared response and to the relative decrease in its red reflectance in both scattering directions (Fig. 11). Thus differences in magnitude in both seasons may be related not only with phenologic aspects but also with sun-view-angle effects. These results are in agreement with previous studies that investigated NDVI variations according to sun-view-angle changes with decreasing LAI (Walter-Shea et al., 1997, Liesenberg et al., 2007) and on the vegetation-type dependence (e.g., Qi et al., 1995, Xavier and Galvão, 2005).

**View-Angle Effects on Discrimination Performance**

In Principal Component (PC) space, small differences between the scores indicate spectral similarity between the classes. The dispersion of the PC scores in both seasons for the forest types tends to be greater in the backward direction (closed symbols) than in the forward direction (open symbols), whereas for the grassland classes the dispersion was greater at nadir and in the forward direction. To indicate the best view direction to enhance discrimination between pairs of classes, the first PC score differentiates between ASF and DRG, and GSL and SHL were plotted as a function of view angles in both seasons (Fig. 12). At a given direction small PC score differences indicate spectral similarity between the two classes, whereas large differences indicate dissimilarity.

The best direction for the discrimination of the two forest types (e.g., ASF and DRG) was verified at the +36° for the image collected at the end of the monsoon and +55° view angle for the image collected at the beginning of the dry season (backward direction). The smallest PC1 differences were observed at these angles. Less favorable viewing conditions were found at nadir and in the forward scattering direction at the view-shading condition (e.g., –36° view angle).

Figure 13 illustrates the classification accuracy results from MDA for each class, view angle, and date. For a single view-angle perspective (e.g., at nadir), classification accuracy values at the end of the monsoon were slightly higher than those obtained at the beginning of the dry season (Tables 2 and 3). For the image collected at the end of the monsoon, the classification accuracy generally increases from the forward- (negative view angles) to the backward- (positive view angles) scattering direction (Fig. 13A) and from the backward to the forward scattering direction in the dry season (Fig. 13B). However, in both images there were still some poorly discriminated classes that required a multi-angular approach to improve classification.

Overall classification accuracy improves from 77% (nadir; Table 2) to 90% (multi-angular; Table 3) for the image acquired at the end of the monsoon, as opposed to 59% (nadir; Table 4) to 93% (multi-angular; Table 5) at the beginning of the dry season.
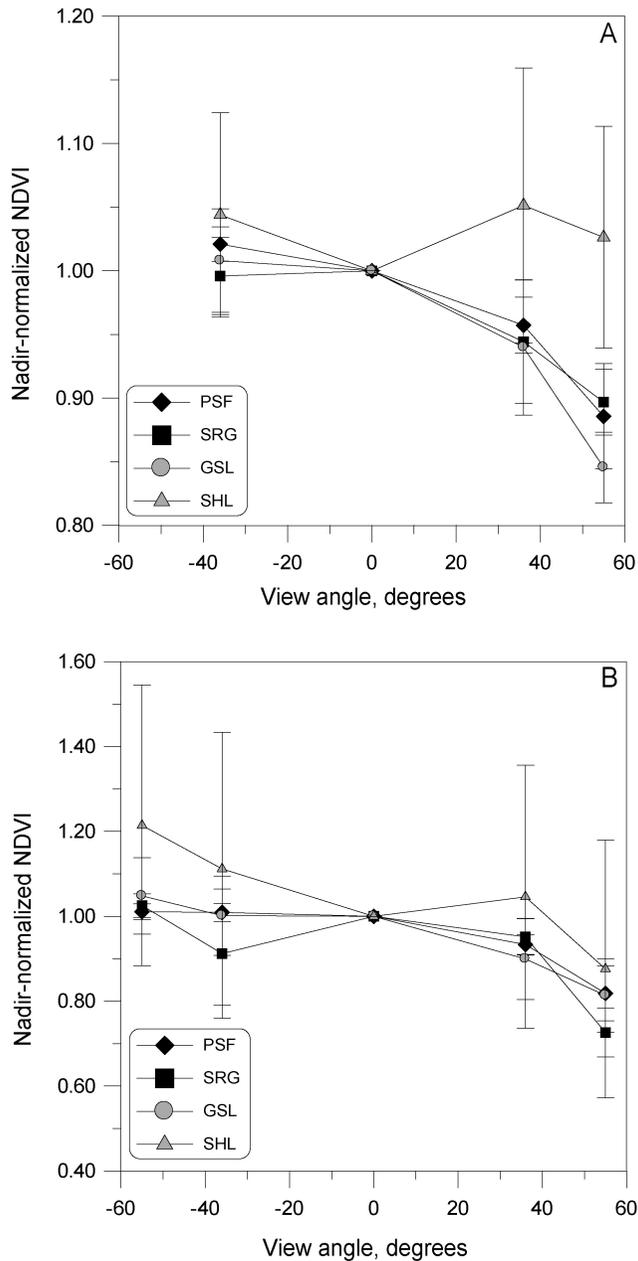
**Fig. 11.** Angular variations in nadir-normalized NDVI angular profiles of different tropical peat swamp classes for (A) May 18, 2004 and (B) June 06, 2006. Average and standard deviation of 40 pixels. Refer to Figure 2 for the selected class's category.

Compared to a single-view-angle approach (e.g., nadir) the use of a multi-angular approach increased the accuracy of most of the selected classes on both dates. Dense regrowth is the only class whose individual accuracy decreases from 63% to 59% at

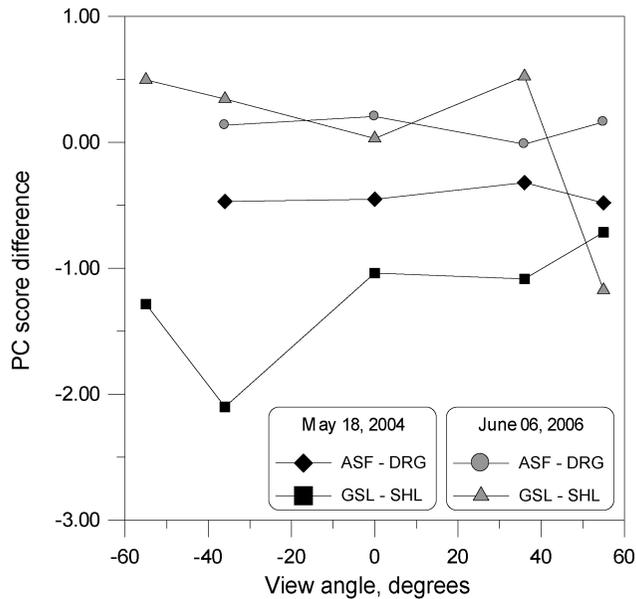**Fig. 12.** Differences of the first principal component scores (PC1; average and standard deviation of 40 pixels) as a function of view angles between pairs of classes (e.g. ASF and DRG, GSL and SHL). Large score differences indicate dissimilarity. Refer to Figure 2 for the selected class's category.

**Table 2.** Error Matrix for Single-View-Angle Approach (at nadir 2004)[a]

|       | Reference data | | | | | | | |
|-------|------|------|------|------|-------|------|------|------|
|       | PSF  | ASF  | DRG  | SRG  | SHL   | GSL  | WTL  | BRT  |
| PSF   | 70.3 |      |      |      |       | 29.7 |      |      |
| ASF   | 4.5  | 80.0 | 3.0  |      |       | 12.5 |      |      |
| DRG   | 2.5  | 20.7 | 63.5 | 1.7  |       | 11.5 |      |      |
| SRG   |      | 1.3  | 13.7 | 85.0 |       |      |      |      |
| SHL   |      |      |      |      | 100.0 |      |      |      |
| GSL   | 11.5 | 18.0 |      |      |       | 63.7 | 5.3  | 1.5  |
| WTL   |      |      |      |      |       |      | 64.7 | 35.3 |
| BRT   |      |      |      |      |       | 1.7  | 8.5  | 89.7 |

[a]Values are indicated in percentage values. Overall accuracy was 77% (Kappa index = 0.74).

the end of the monsoon. In the beginning of the dry season a decrease of individual accuracy was observed for sparse regrowth (80% to 77%).

Misclassification between classes as well as the small decrease of the individual classification accuracy for the aforementioned classes may be related to the small variability of LAI between them and regrowth effects that are more enhanced for initial
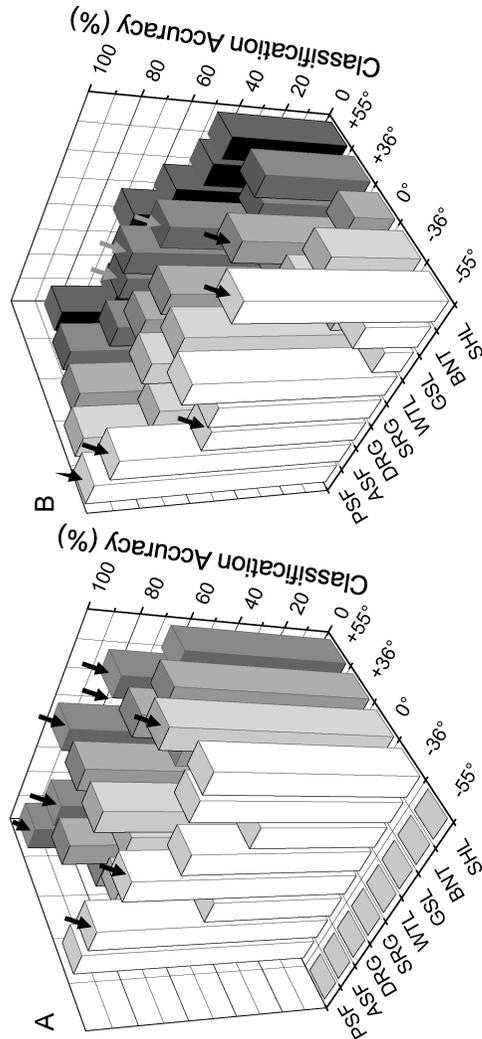
**Fig. 13.** Variations in classification accuracy values with view angle changes for (A) May 18, 2004 and (B) June 06, 2006 for all the classes under study. View angles with the best classification accuracy are indicated by arrows. Refer to Figure 2 for the selected class's category.

**Table 3.** Error Matrix for Multi-angular Approach (all view angles 2004)[a]

| | Reference data | | | | | | | |
|---|---|---|---|---|---|---|---|---|
| | PSF | ASF | DRG | SRG | SHL | GSL | WTL | BRT |
| PSF | 99.7 | 0.3 | | | | | | |
| ASF | 3.5 | 96.3 | | 0.3 | | | | |
| DRG | 9.0 | 15.7 | 59.7 | 13.0 | | 2.5 | | |
| SRG | | 1.7 | 1.0 | 97.3 | | | | |
| SHL | | | | | 100.0 | | | |
| GSL | | | 0.3 | 0.3 | | 94.7 | 4.5 | 0.3 |
| WTL | | | | | | | 87.0 | 13.0 |
| BRT | | | 0.5 | | | 2.7 | 8.3 | 88.5 |

[a]Values are indicated in percentage values. Overall accuracy was 90% (Kappa index = 0.89).

**Table 4.** Error Matrix for Single-View-Angle Approach (at nadir 2006)[a]

| | Reference data | | | | | | | |
|---|---|---|---|---|---|---|---|---|
| | PSF | ASF | DRG | SRG | SHL | GSL | WTL | BRT |
| PSF | 92.5 | 5.0 | | | | 2.5 | | |
| ASF | 25 | 57.5 | 2.5 | 15.0 | | | | |
| DRG | | | 62.5 | 27.5 | | 7.5 | 2.5 | |
| SRG | | 5.0 | 12.5 | 80.0 | | 2.5 | | |
| SHL | | | | | 75.0 | 2.5 | 20.0 | 2.5 |
| GSL | | | 20.0 | 7.5 | 7.5 | 35.0 | 20.0 | 10.0 |
| WTL | | | | | 12.5 | 17.5 | 57.5 | 12.5 |
| BRT | | | | | | 27.5 | 55.0 | 17.5 |

[a]Values are indicated in percentage values. Overall Accuracy was 59% (Kappa index = 0.54).

succession classes (Vieira et al., 2003). Interestingly, there is better differentiation using multi-angular data between secondary succession classes. These are reported as the most difficult to be mapped in the Amazonian environment (Lucas et al., 2000, 2002; Lu et al., 2003).

Results from both the McNemar and Z-test confirmed that the multi-angular approach produced statistically better classification values at a 1% level of significance to better differentiate the classes than nadir viewing for both images (single-view-angle approach) (Table 6). The additional use of shortwave infrared (SWIR) data is pointed out by different researchers (e.g., Lucas et al., 2002; Vieira et al., 2003) as being very useful for discrimination purposes as well as the retrieval of biophysical properties in tropical environments (e.g., Lu et al., 2004; Wijaya et al., 2010). Unfortunately CHRIS/PROBA cannot collect SWIR information, but this capability

**Table 5.** Error Matrix for Multi-angular Approach (all view angles 2006)[a]

| | Reference data | | | | | | | |
| | PSF | ASF | DRG | SRG | SHL | GSL | WTL | BRT |
|---|---|---|---|---|---|---|---|---|
| PSF | 100.0 | | | | | | | |
| ASF | 7.5 | 90.0 | | 2.5 | | | | |
| DRG | | | 90.0 | 5.0 | | 2.5 | 2.5 | |
| SRG | | 7.5 | 15.0 | 77.5 | | | | |
| SHL | | | | | 92.5 | 5.0 | | 2.5 |
| GSL | | | | | | 95.0 | 5.0 | |
| WTL | | | | | | | 97.5 | 2.5 |
| BRT | | | | | | | | 100.0 |

[a]Values are indicated in percentage values. Overall Accuracy was 93% (Kappa index = 0.92).

**Table 6.** Summary of the (A) Z-test and (B) McNemar Test for Comparison of Overall Accuracy of CHRIS/PROBA in Single-View-Angle Approach (at nadir) and Multi-angular Approach (all view angles)

| | Multi-angular approach | |
| | 2004 | 2006 |
|---|---|---|
| A. Z-test | | |
| Single-view-angle approach | 14.7 | 10.9 |
| B. McNemar test | | |
| Single-view-angle approach | 11.9 | 5.9 |

is expected from the Environmental Mapping and Analysis Program (EnMap) in the near future (Stuffler et al., 2007).

Although the analysis is restricted to selected pixels in two distinct periods, it leads to a better understanding of the anisotropy influence on the spectral discrimination of peat swamp forest classes. While the potential of multi-angular information for entire scenes still has to be evaluated, similar results will likely be obtained if other classes besides those used in this investigation are masked and not considered in the analysis. Additional classes such as pasture, crops, and urban areas that are also present in the study area showed different reflectance anisotropy patterns to those evaluated in this study.

## CONCLUSIONS

In relation to nadir view angle the strongest anisotropy was observed in the backward-scattering direction, in which great amounts of sunlit canopy components were viewed by the sensor. Such effects were more intense in the visible bands than in the

near infrared. Peat swamp forest and grassland were the classes that showed the highest anisotropy, especially for the red band due to its higher LAI values and scattering effects.

Near infrared reflectance (NIR) increased from burned areas to shrubs and grassland to the successional stages for a given angle and date. The successional forest also presented large reflectance values in NIR with decreasing leaf area index (LAI) and less well structured canopy layers. The spectral behavior between peat swamp forest and successional stages showed similar trends to those observed in distinct tropical environments in the Amazon biome. Phenologic patterns were observed for the selected classes and reflectance changes were slightly positive for forestry classes whereas slightly negative for grassland classes.

Atmospheric dispersion in the blue region was still noticed even after correction, suggesting a fail in radiative transfer codes for the tropical atmosphere mode and mainly the backward-scattering direction. NDVI variations were stronger in distinct view angles for shrubland than for the remaining classes and decreased for the forestry classes. Forestry classes showed similar shapes in the principal component space over time due to higher LAI values.

In comparison to the single-view-angle approach (nadir) the multi-angular approach produced an overall discrimination improvement for both selected dates. According to the *Z* and McNemar tests, the differences between the two classifications (nadir and multi-angular) on the selected dates were statistically significant at a 1% level of significance.

Nonetheless, further research is necessary in order to test the performance of other classification methods and feature selection techniques in terms of differentiating between vegetation types in Indonesia. There is much potential for the additional use of shortwave infrared (SWIR) multi-angular data, which unfortunately cannot be collected by the CHRIS/PROBA. This information will be collected by the forthcoming Environmental Mapping and Analysis Program (EnMap).

## ACKNOWLEDGMENTS

## REFERENCES

Abdou, W. A., Helmlinger, M. C., Conel, J. E., Bruegge, C. J., Pilorz, S. H., Martonchik, J. V., and B. J. Gaitley, 2000, "Ground Measurements of Surface BRF and HDRF Using PARABOLA III," *Journal of Geophysical Research-Atmospheres*, 106(D11):11,967–11,976.

Barnsley, M. J., Settle, J. J., Cutter, M. A., Lobb, D. R., and F. Teston, 2004, "The PROBA/CHRIS mission: A low-cost Smallsat for Hyperspectral Multi-angle Observations of the Earth Surface and Atmosphere," *IEEE Transactions on Geosciences and Remote Sensing*, 42(7):1512–1520.

Boehm, H-D. V., Ramirez, S., and D. Bustillo, 2005, "Environmental Management Study of the Tangkilling District along River Rungan in Central Kalimantan, using Remote Sensing and GIS," Yogyakarta, Indonesia, Open Science Meeting.

Brearley, F. Q., Prajadinata, S., Kidd, P. S., Proctor, J., and Suriantata, 2004, "Structure and Floristics of an Old Secondary Rain Forest in Central Kalimantan, Indonesia, and a Comparison with Adjacent Primary Forest," *Forest Ecology and Management*, 195(3):385–397.

Carreiras, J. M. B., Pereira, J. M. C., Campagnolo, M. L., and Y. E. Shimabukuro, 2006, "Assessing the Extent of Agriculture/Pasture and Secondary Succession Forest in the Brazilian Legal Amazon Using SPOT Vegetation Data," *Remote Sensing of Environment*, 101(3):283–298.

Congalton, R. and K. Green, 1999, *Assessing the Accuracy of Remotely Sensed Data: Principles and Practices*, Boca Raton, FL: CRR/Lewis Press, 137 p.

Diner, D. J., Asner, G. P., Davies, R., Knyazikhin, Y., Muller, J. P., Nolin, A. W., Pinty, B., Schaaf, C. B., and J. Stroeve, 1999, "New Directions in Earth Observing: Scientific Applications of Multi-angle Remote Sensing," *Bulletin of the American Meteorological Society*, 80(11):2209–2228.

Felde, G. W., Anderson, G. P., Cooley, T. W., Matthew, M. W., Adler-Golden, S. M., Berk, A., and J. Lee, 2003, "Analysis of Hyperion Data with the FLAASH Atmospheric Correction Algorithm," *Proceedings of the International Geoscience and Remote Sensing Symposium, Toulouse, France, 2003 (IGARSS'03)*, 90–92.

Foody, G. M., Palunbiskas, G., Lucas, R. M., Curran, P. J., and M. Honzak, 1996, "Identifying Terrestrial Carbon Sinks: Classification of Successional Stages in Regenerating Tropical Forest from Landsat TM Data," *Remote Sensing of Environment*, 55(3):205–216.

Galvão, L. S., Ponzoni, F. J., Liesenberg, V., and J. R. Santos, 2009, "Possibilities of Discriminating Tropical Secondary Succession in Amazônia Using Hyperspectral and Multiangular CHRIS/PROBA data," *International Journal of Applied Earth Observation and Geoinformation*, 11(1): 8–14.

Guanter, L., Alonso, J., and J. Moreno, 2005, "First results from the PROBA/CHRIS Hyperspectral/Multiangular Satellite System over Land and Water Targets," *IEEE Geosciences and Remote Sensing Letters*, 2(3):250–254.

Hirano, T., Segah, H., Harada, T., Limin, S., June, T., Hirata, R., and M. Osaki, 2007, "Carbon Dioxide Balance of a Tropical Peat Swamp Forest in Kalimantan, Indonesia," *Global Change Biology*, 13(2): 412–425.

Huberty, C. J., 1984, "Issues in the Use and Interpretation of Discriminant Analysis," *Psychological Bulletin*, 95(1):156−171.

Huete, A. R., Didan, K., Shimabukuro, Y. E., Ratana, P., Saleska, S. R., Hutyra, L. R., Yang, W., Nemani, R. R., and R. Myneni, 2006, "Amazon Rainforests Green-up with Sunlight in the Dry Season," *Geophysical Research Letters*, 33, L06405.

Huete, A. R., Kim, Y., Ratana, P., Didan, K., Shimabukuro, Y. E., and T. Miura, 2008, "Assessment of Phenologic Variability in Amazon Tropical Rainforests Using Hyperspectral Hyperion and MODIS Satellite Data, in *Hyperspectral Remote*

*Sensing of Tropical and Sub-Tropical Forests*, London: CRC Press Inc., 233–259.

Jaenicke, J., Rieley, J. O., Mott, C., Kimman, P., and F. Siegert, 2008, "Determination of the Amount of Carbon Stored in Indonesian Peatlands," *Geoderma*, 147(3–4):151–158.

Jauhiainen, J., Takahashi, H., Heikkinen, J. E. P., Martikainen, P. J., and H. Vasander, 2005, "Carbon Fluxes from a Tropical Peat Swamp Forest Floor," *Global Change Biology*, 11(10):1788–1797.

Jensen, J. R., 2005, *Introductory Digital Image Processing*, 3rd ed., Upper Saddle River, NJ: Prentice Hall: 526 pp.

Kimes, D. S., Harrison, P. A., and P. R. Harrison, 1994, "Extension of Off-Nadir View Angles for Directional Sensor Systems," *Remote Sensing of Environment*, 50(3): 201–211.

Kimes, D. S., Nelson, R. F., Salas, W. A., and D. L. Skole, 1999, "Mapping Secondary Tropical Forest and Forest Age from SPOT HRV Data," *International Journal of Remote Sensing*, 20(18): 3625–3640.

Liesenberg, V., Galvão, L. S., and F. J. Ponzoni, 2007, "Variations in Reflectance with Seasonality and Viewing Geometry: Implications for Classification of Brazilian Savanna Physiognomies with MISR/Terra Data," *Remote Sensing of Environment*, 107(1–2):276–286.

Lu, D., 2005, "Integration of Vegetation Inventory Data and Landsat TM Image for Vegetation Classification in Western Brazilian Amazon," *Forest Ecology and Management*, 213(1–3): 369–383.

Lu, D., Mausel, P., Brondízio, E., and E. Moran, 2003, "Classification of Successional Forest Stages in the Brazilian Amazon Basin," *Forest Ecology and Management*, 181(3):301–312.

Lu, D., Mausel, P., Brondizio, E., and E. Moran, 2004, "Relationships between Forest Stand Parameters and Landsat TM Spectral Responses in the Brazilian Amazon Basin," *Forest Ecology and Management*, 198(1–3): 149–167.

Lucas, R. M., Honzák, M., Amaral, I. D., Curran, P. J., and G. M. Foody, 2002, "Forest Regeneration on Abandoned Clearances in Central Amazonia," *International Journal of Remote Sensing*, 23(5):965–988.

Lucas, R. M., Honzák, M., Curran, P. J., Foody, G. M., Milnes, R., Brown, T., and S. Amaral, 2000, "Mapping the Regional Extent of Tropical Forest Regeneration Stages in the Brazilian Legal Amazon Using NOAA AVHRR data," *International Journal of Remote Sensing*, 21(15):2855–2881.

Lucas, R. M., Honzak, M., Foody, G. M., Curran, P. J., and C. Corves, 1993, "Characterizing Tropical Secondary Forests Using Multitemporal Landsat Sensor Imagery," *International Journal of Remote Sensing*, 14(16):3061–3067.

Nishimua, T. B., Suzuki, E., Kohyama, T., and S. Tsuyuzaki, 2007, "Mortality and Growth of Trees in Peat-Swamp and Heath Forests in Central Kalimantan after Severe Drought," *Plant Ecology*, 188(2):165–177.

Page, S. E., Siegert, F., Rieley, J. O., Boehm, H-D. V., Jaya, A., and S. Limin, 2002, "The Amount of Carbon Released from Peat and Forest Fires in Indonesia during 1997," *Nature*, 420(6911):61–65.

Page, S. E., Rieley, J. O., Shotyk, Ø. W., and D. Weiss, 1999, "Interdependence of Peat and Vegetation in a Tropical Peat Swamp Forest," *Philosophical Transactions: Biological Sciences*, 354(1391):1885–1897.

Qi, J., Moran, M. S., Cabot, F., and G. Dedieu, 1995, "Normalization of Sun/View Angle Effects Using Spectral Albedo-Based Vegetation Indices," *Remote Sensing of Environment*, 52(3):207–217.

Reif, M., Frohn, R. C., Lane, C. R., and B. Autrey, 2009, "Mapping Isolated Wetlands in a Karst Landscape: GIS and Remote Sensing Methods," *GIScience & Remote Sensing*, 46(2): 187–211, 2009.

Sandmeier, S. T. and D. W. Deering, 1999, "Structure Analysis and Classification of Boreal Forests Using Airborne Hyperspectral BRDF Data from ASAS," *Remote Sensing of Environment*, 69(3):281–295.

Sandmeier, S. T., Müller, C., Hosgood, B., and G. Andreoli, 1998, "Physical Mechanisms in Hyperspectral BRDF Data of Grass and Watercress," *Remote Sensing of Environment* 66(2):222–233.

Schaepman-Strub, G., Schaepman, M. E., Painter, T. H., Dangel, S., and J. V. Martonchik, 2006, "Reflectance Quantities in Optical Remote Sensing—Definitions and Case Studies," *Remote Sensing of Environment*, 103(1):27–42.

Schill, S., Jensen, J. R., Raber, G., and D. E. Porter, 2004, "Temporal Modeling of Bidirectional Reflection Distribution Function (BRDF) in Coastal Vegetation," *GIScience & Remote Sensing*, 41(2):116–135.

Stuffler, T., Kaufmann, C., Hofer, S., Foerster, K. P., Schreier, G., Mueller, A., Eckardt A., Bach, H., Penne, B., Benz, U., and R. Haydn, 2007, "The EnMAP Hyperspectral Imager—An Advanced Optical Payload for Future Applications in Earth Observation Programmes," *Acta Astronautica*, 61(1–6):115–120.

Twelle, A., Erasmi, S., and M. Kappas, 2008, "Spatially Explicit Estimation of Leaf Area Index Using EO-1 Hyperion and Landsat ETM+ Data: Implications of Spectral Bandwidth and Shortwave Infrared Data on Prediction Accuracy in a Tropical Montane Environment," *GIScience & Remote Sensing*, 45(2):229–248.

Usup, A., Hashimoto, Y., Takahashi, H., and H. Hayasaka, 2004, "Combustion and Thermal Characteristics of Peat Fire in Tropical Peatland in Central Kalimantan, Indonesia," *Tropics*, 14(1):1–19.

Vieira, I. C. G., Almeida, A. S., Davidson, E. A., Stone, T. A., Carvalho, C. J. R., and J. B. Guerrero, 2003, "Classifying Successional Forests Using Landsat Spectral Properties and Ecological Characteristics in Eastern Amazônia," *Remote Sensing of Environment*, 87(4):470–481.

Walter-Shea, E. A., Privette, J., Cornell, D., Mesarch, M. A., and C. J. Hays, 1997, "Relations between Directional Spectral Vegetation Indices and Leaf Area and Absorbed Radiation in Alfalfa," *Remote Sensing of Environment*, 61(1):162–177.

Wijaya, A., Liesenberg, V., and R. Gloaguen, 2010, Retrieval of Forest Attributes in Complex Successional Forest of Central Indonesia: Modeling and Estimation of Bitemporal Data," *Forest Ecology and Management*, 259(12):2315–2326.

Xavier, A. S. and L. S. Galvão, 2005, "View Angle Effects on the Discrimination of Selected Amazonian Land Cover Types from a Principal-Component Analysis of MISR Spectra," *International Journal of Remote Sensing*, 26(17):3797–3811.

Zhang, Y., Tian, Y., Myneni, R. B., Knyazikhin, Y., and C. E. Woodcock, 2002, "Assessing the Information Content of Multiangle Satellite Data for Mapping Biomes: I. Statistical Analysis," *Remote Sensing of Environment*, 80(3):418–434.